Chapter 2
Fundamentals of Vehicle Modeling

At least three energy conversion steps are relevant for a comprehensive analysis of energy efficiency of passenger cars and other road vehicles. As illustrated in Fig. 2.1, in a first step ("*grid-to-tank*"), energy carriers that are available at stationary distribution networks, such as gasoline, electricity, etc., are transferred to an on-board storage system. This energy is then converted by the propulsion system to mechanical energy aimed at propelling the vehicle (‘"*tank-to-wheels*"). In the third energy conversion step ("*wheel-to-distance*"), this mechanical energy is ultimately converted into the kinetic and potential energy required by the displacement. Unfortunately, all of these conversion processes may cause substantial energy losses.

Tank-to-wheels efficiency may be improved by several approaches, both at the component level and at the system control level [1]. Methods to improve grid-to-tank efficiency by choosing the appropriate charging time slots and profiles are currently being studied for electric vehicles. The maximization of wheel-to-distance efficiency is one of the main topics of this book. Although minimizing the energy at wheels E_W for a given amount of the useful energy E_M is theoretically possible and will be actually treated in the following chapters, it is often more interesting to try to minimize the energy consumed by the on-board sources ("tanks"), E_T. To analyze such a problem, we shall introduce in the following section vehicle-specific models of powertrain components.

The standard tool to evaluate tank-to-distance efficiency and predict energy consumption of road vehicles as a function of how they are driven is the use of modular modeling of the vehicle and its propulsion system. As Figs. 2.2, 2.3, 2.4, 2.5 and 2.6 suggest, such models are composed of several sub-models representing each relevant energy conversion step from E_T to E_M. To evaluate the tank energy for a given driving profile, these models are typically solved "backwards", i.e., the model inputs are at the road level (speed, acceleration), and the energy conversion chain is followed in the opposite direction of the physical energy flow, to eventually evalu-

A. Sciarretta and A. Vahidi, *Energy-Efficient Driving of Road Vehicles*,
Lecture Notes in Intelligent Transportation and Infrastructure,
https://doi.org/10.1007/978-3-030-24127-8_2

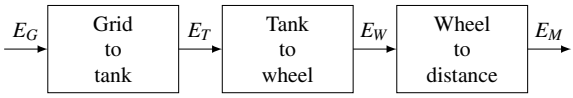

Fig. 2.1 Macroscopic energy conversion steps in road transport

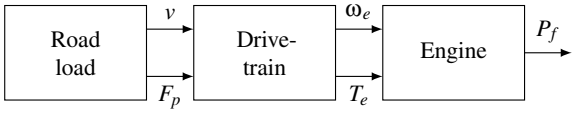

Fig. 2.2 Backward calculation of energy consumption rate in an engine-powered vehicle. Nomenclature defined in Sects. 2.1–2.2

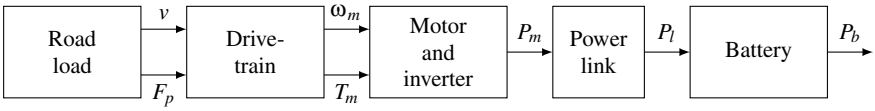

Fig. 2.3 Backward calculation of energy consumption rate in an electric vehicle. Nomenclature defined in Sect. 2.3

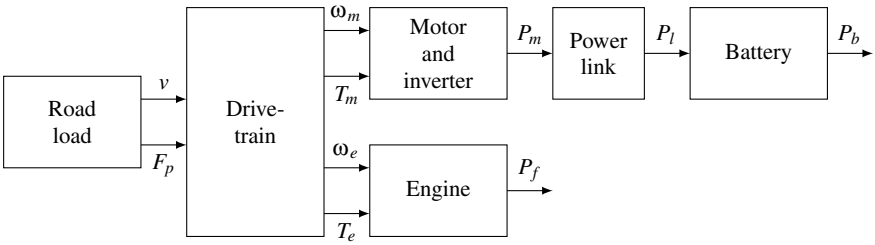

Fig. 2.4 Backward calculation of energy consumption rate in a parallel hybrid-electric vehicle. Nomenclature defined in Sect. 2.4

ate the power drained from on-board sources. In contrast, the physical energy flow (from the sources to the road) is followed to predict the effects of powertrain control strategies on driving and, consequently, on energy consumption. For this purpose, the same modular approach of Figs. 2.2, 2.3, 2.4, 2.5 and 2.6 can be used, albeit with physical causality ("forward" modeling).

In Sect. 2.1, a model for the energy required at the wheels that is common to all types of road vehicles is presented. Then, each propulsion system is modeled separately, and the main equations that are useful to evaluate the tank energy consumption are summarized (Sect. 2.2–2.5).

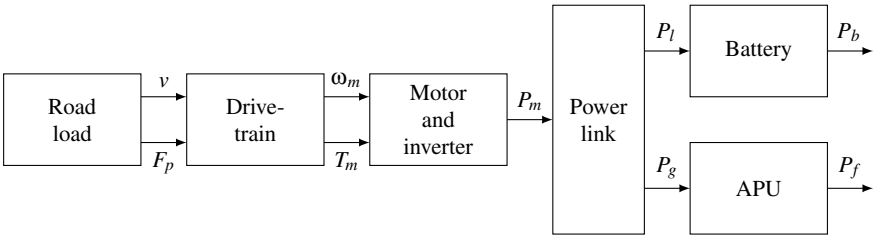

Fig. 2.5 Backward calculation of energy consumption rate in a series hybrid-electric vehicle. Nomenclature defined in Sect. 2.4

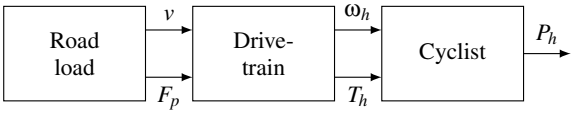

Fig. 2.6 Backward calculation of energy consumption rate in an human-powered vehicle. Nomenclature defined in Sect. 2.5

2.1 Road Load

From a dynamic viewpoint, road vehicles are generally treated as semi-rigid bodies and described by their linear and angular position along three coordinated dimensions. For our purposes, however, the longitudinal motion often suffices.[1] We shall therefore consider the dynamics of longitudinal position, $s(t)$, and speed, $v(t) \triangleq \dot{s}(t)$.

2.1.1 Forces Acting on Road Vehicles

The vehicle's longitudinal dynamics is governed by Newton's second law of motion, see Fig. 2.7,

$$m_t \frac{dv(t)}{dt} = F_p(t) - F_{\text{res}}(t) - F_b(t) \ . \tag{2.1}$$

In this equation, $m_t = m + m_r$ is *total effective mass*, sum of the overall mass m of the vehicle (curb mass) and of its occupants, plus a term m_r that describes the effect of the inertia of rotating parts (engine, motor, etc.) transferred to the wheels. The latter term is usually varying with time as transmission ratio changes, but this variation is often neglected. Of course, vehicle mass has a wide range, from less than 100 kg for bicycles (where the cyclist's mass is prominent over the vehicle) to several thousand kg for heavy-duty trucks.

[1] Even in the presence of lateral maneuvers such as lane changes (see, e.g., Sect. 9.4), the energy consumption associated with such transient maneuvers will be neglected.

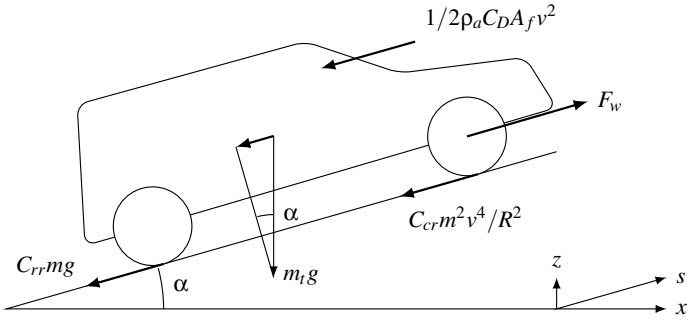

Fig. 2.7 Schematic representation of the forces acting on a vehicle in motion

The force F_p is the sum of forces applied by the powertrain at the wheels, as explained below. The term F_b is the force applied by frictional brakes only, while "regenerative" brake possibly provided by electric, hydraulic, pneumatic, or kinetic means coupled with accumulators is considered here as part of the propulsion system.

The term representing road load, F_{res}, may include several contributions. Limiting our analysis to the most relevant ones, we shall write the road load as

$$F_{\text{res}}(t) = \frac{1}{2}\rho_a C_D(t) A_f \left(v(t) - w\right)^2 + C_{rr} mg \cos(\alpha(s(t))) + \\ + C_{cr} \frac{m^2 v(t)^4}{R(s(t))^2} + mg \sin(\alpha(s(t))) \,, \tag{2.2}$$

where C_{rr} is the coefficient of rolling resistance, α and R are the road slope and the out-of-the-pictured-plane radius of curvature, which are generally functions of the vehicle's position s, ρ_a is air density, w is longitudinal wind speed, A_f is vehicle's frontal area, C_{cr} the coefficient of cornering resistance [2, 3], and C_D is the aerodynamic drag coefficient.

The first three terms in the right-hand side of (2.2) must be regarded as approximations of physically complex phenomena [1]. Basically, these terms define the coefficients C_{rr}, C_{cr}, and C_D to represent rolling, cornering, and aerodynamic resistance forces. Typical values for C_{rr} on dry roads range from 0.002 (high-quality bicycle racing tires) to 0.02 (car tires at low pressure). Typical values for C_D range from 0.15 (low-drag concept cars) to 1.2 (utility bicycles with cyclist). The order of magnitude of C_{cr} is of 10^{-5}.

The main factors that influence such parameters are described in standard books on vehicle systems [1]. They comprise of vehicle, road, and weather factors, such that for a given trip, they can be generally considered as constants.[2] Perhaps the only relevant exception is the variation of C_D as a function of the inter-distance with a leading vehicle. Since the reduction of this coefficient when the inter-distance approaches to

[2]From here on, we shall always make use of this assumption, unless explicitly stated.

zero can be very relevant, both for the follower and, albeit less markedly, the leader [4, 5], this property is the basis of energy-saving techniques such as platooning (for heavy-duty trucks) or drafting (for bicycles).

Often F_{res} is identified as a whole by letting the vehicle coast ($F_p = F_b = 0$) on a flat and straight road ($\alpha = 0$, $R \to \infty$) with no wind ($w = 0$), and observing the speed variation, then expressed as a polynomial function of $v(t)$,

$$F_{\text{res}}(t) = C_0 + C_1 v(t) + C_2 v(t)^2 \ , \tag{2.3}$$

where the C's are called the *road load coefficients*.

Note that, in the "backward" approach presented at the beginning of this chapter, (2.1)–(2.3) are used to evaluate $F_p(t)$ as a function of $v(t)$, its derivative dv/dt, and $s(t)$.

2.1.2 Energy Requirement at the Wheels

Based on the longitudinal dynamics introduced in the previous section, in this section we shall derive equations for the energy needed at the wheels, E_W, to follow a prescribed speed profile $v(t)$ covering a distance s_f in t_f units of time. For such a "trip", the useful energy E_M will be defined as

$$E_M = \frac{1}{2} m_t (v_f^2 - v_i^2) + mg\Delta z \ , \tag{2.4}$$

where v_i and v_f are velocities at origin and destination respectively, and Δz is total elevation change during the trip.

Let us first define the net force at the wheels as $F_w(t) \triangleq F_p(t) - F_b(t)$. The instantaneous power needed at the wheels is thus $F_w(t)v(t)$. From (2.1–2.2), assuming a straight road with no wind,[3] the net energy E_W can then be calculated as

$$E_W = \int_0^{t_f} F_w(t)v(t)dt = \int_0^{t_f} \left(m_t \frac{dv(t)}{dt} + mg(sin\alpha(s(t)) + C_{rr} cos\alpha(s(t)) + \frac{1}{2}\rho_a A_f C_D v^2(t) \right) v(t)dt \ . \tag{2.5}$$

Using (2.4), integration yields

$$E_W = E_M + mgC_{rr}\Delta x + \frac{1}{2}\rho_a A_f C_D \int_0^{t_f} v^3(t)dt \ , \tag{2.6}$$

[3] From here on, we shall always make use of this assumption, unless explicitly stated.

where Δx is the horizontal distance covered. Note that road grade does not appear after integration. However, it shall be explained later that, because of constraints on velocity and powertrain output, the elevation profile along a trip can have a significant effect on energy use and prior knowledge of it can help save fuel via better constraint management.

The analysis of (2.6) shows that the term E_M does not offer opportunities for reducing E_W, since it is dictated by initial and terminal conditions only. The term $mgC_{rr}\Delta x$ represents the irreversible frictional loss and could be reduced by choosing shorter routes with lower C_{rr}. The last term, the energy lost to aerodynamic drag, is the only term that can be influenced by the decisions along the route and therefore should be a core consideration in eco-driving.

In this regard, lower speeds obviously result in lower losses to drag. More specifically, the drag term can be explicitly evaluated as in [6]:

$$\frac{1}{2}\rho_a A_f C_D \int_0^{t_f} v^3(t)dt = \frac{1}{2}\rho_a A_f C_D \left(\frac{b_v \sigma_v^3}{\bar{v}} + 3\sigma_v^2 + \bar{v}^2\right) s_f \ , \tag{2.7}$$

where

$$\bar{v} \triangleq \frac{\int_0^{t_f} v(s)dt}{t_f} = \frac{s_f}{t_f} \ , \tag{2.8}$$

is the average speed (first raw moment of speed),

$$\sigma_v^2 \triangleq \frac{\int_0^{t_f} (v(t) - \bar{v})^2 dt}{t_f} \ , \tag{2.9}$$

is its variance (second central moment), and

$$b_v \triangleq \frac{\int_0^{t_f} (v(t) - \bar{v})^3 dt}{t_f \sigma_v^3} \ , \tag{2.10}$$

is speed skewness (third standardized moment). A generalization of (2.6) with the parametrization (2.3) for the flat road load thus reads

$$E_W = E_M + \left(C_0 + C_1\bar{v} + C_2\bar{v}^2 + C_1\frac{\sigma_v^2}{\bar{v}} + 3C_2\sigma_v^2 + \frac{C_2 b_v \sigma_v^3}{\bar{v}}\right) s_f \ . \tag{2.11}$$

In summary, the wheel-to-distance energy loss $E_W - E_M$ depends on four driving parameters (s_f, $\bar{v}$ or, alternatively, t_f, σ_v^2, and b_v) and three vehicle parameters (C_0, C_1, C_2). Their relative influence can be evaluated with a sensitivity analysis, defining the sensitivity with respect to the generic parameter π as

$$S_\pi \triangleq \frac{\partial(E_W - E_M)}{\partial \pi} \cdot \frac{\pi}{E_W - E_M} \ . \tag{2.12}$$

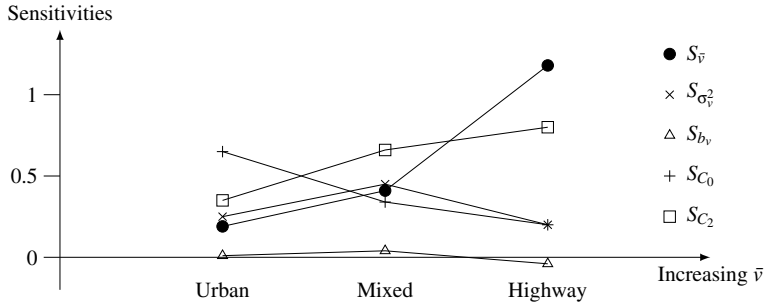

Fig. 2.8 Relative influence of driving profile parameters on the wheel-to-distance losses of a typical full-size passenger car, for urban, mixed, and highway type profiles

Typical values of sensitivities to driving and vehicle parameters are shown in Fig. 2.8 for urban, mixed, and highway driving profiles. While the influence of C_0 (largely representative of rolling resistance) is larger than that of C_2 (aerodynamic drag) at low average speeds, the situation is the opposite as $\bar{v}$ increases. For high average speeds, the relative influence of $\bar{v}$ also becomes dominant over that of the other driving parameters. The sensitivity $\bigotimes_{\sigma_v^2}$ is only relevant for urban and mixed driving conditions. Finally, the skewness b_v has generally a little influence.

The previous analysis shows that, while vehicle parameters play an important role in determining the energy demand, the approach of improving wheel-to-meters efficiency by "controlling" the driving profile reveals all its potential when considering that it does not require structural or material changes to the system.

2.1.3 Energy Required from the Powertrain

The wheel energy evaluated with (2.6) or (2.11) does not take into account the energy dissipated in friction brakes that are acting on the wheels. To include this term, *powertrain energy* can be defined as

$$E_p = \int_0^{t_f} F_p(t)v(t)dt = E_W + \int_0^{t_f} F_b(t)v(t)dt \ , \tag{2.13}$$

where the braking force $F_b \geq 0$ explicitly appears.

The amount of this force (total braking effort) depends on the braking strategy and is usually split between the wheel axles. Of course, brakes are normally activated only for slowing a moving vehicle, thus to provide a required deceleration in addition to that induced by resistive forces. For our purposes, it is reasonable to assume that

$$F_b(t) = \begin{cases} -(1 - k_b(t))F_w(t), & \text{if } F_w(t) < 0 \\ 0, & \text{otherwise} \end{cases}, \tag{2.14}$$

where k_b is the *ratio of regenerative braking* force (recuperated by the powertrain and stored in the onboard tank) to the total braking force. For engine-based vehicles without recuperation devices, k_b is close to zero, while for electrified vehicles $0 < k_b < 1$. An ideal vehicle would have $k_b = 1$ (perfect recuperation) and, in this case, E_p would be the same as E_W.

The condition $F_w < 0$ means that the vehicle transfers power to the powertrain or brakes and defines the *braking mode* $\mathcal{B}$. Contrarily, in the *traction mode* $\mathcal{T}$ (when $F_w > 0$), the vehicle is receiving power from the powertrain. The separating situation is called *coasting*. In such a mode, the vehicle is moving solely due to the resistive forces ($m_t dv/dt = -F_{res}$, $F_w = 0$), thus both F_p and F_b are zero. In the *stop mode* $\mathcal{S}$, if present, the speed is also equal to zero.

Inserting (2.14) into (2.13), the powertrain energy can be evaluated as

$$E_p = \int_{\mathcal{T}} \left(m_t \frac{dv(t)}{dt} + F_{res}(t) \right) v(t)dt + \int_{\mathcal{B}} k_b(t) \left(m_t \frac{dv(t)}{dt} + F_{res}(t) \right) v(t)dt \ . \tag{2.15}$$

The first term in the right-hand side of (2.15) can be explicitly computed with the methods introduced in Sect. 2.1.2, but with the driving parameters (distance, average speed, higher moments) now evaluated for the traction phase only. The second term is negative by definition. Its explicit evaluation is made complex by the variability of k_b. However, if k_b is considered as a constant parameter, the methods of Sect. 2.1.2 still apply.

*
* *

We switch now our attention to the evaluation of the tank energy, that is, the energy consumed from the onboard source(s), differentiating this evaluation by the type of powertrain.

2.2 Internal Combustion Engine Vehicles

Among fuel-powered vehicles, the vast majority are composed of vehicles (cars, trucks, buses, and others) propelled by a reciprocating internal combustion engine (ICE). Such powertrains consists of an engine that burns fuel stored in a tank, delivering mechanical power to a rotating shaft, from which it is transmitted to the wheels by a drivetrain (see Fig. 2.2).

In ICE-powered vehicles (ICEVs), the tank energy consumption corresponds to the chemical energy burned with the fuel,

$$E_T^{(ICEV)} = \int_0^{t_f} P_f(t)dt \ , \tag{2.16}$$

where P_f is the fuel power, the product of fuel mass flow rate and its lower heating value. How P_f is related to the driving profile will be now described by following the approach of Fig. 2.2 and analyzing separately the drivetrain and the engine.

2.2.1 Drivetrain (Gearbox)

In ICE-powered vehicles, the output of the engine is transmitted to the driving wheels by a *drivetrain*. The components in the drivetrain vary according to the type of drive (front-wheel, rear-wheel, four-wheel) but generally include a clutch, a transmission, a drive shaft, and a final drive with differential.

Apart from rarely used continuously-variable transmissions (CVT), usually transmissions with a finite number of gear ratios (*gearboxes*) are used, with the ability to switch between them. The drivetrain transmission ratio γ_e in this case is the product of the transmission ratios of the gearbox and the final drive, and can take the G discrete values $\gamma_e \in \{\gamma_{e,g}\}$, $g = 1, \ldots, G$. The gear selected at a particular time t is determined either by the driver (manual transmissions, automated manual transmissions (AMT)) or by the transmission controller (automatic transmissions). In the latter case, gear ratio is the result of a gear shift law that can be expressed as a map

$$\gamma_e(t) = \Gamma(v(t), F_p(t)) \ . \tag{2.17}$$

A common speed-only-dependent form for such a map is[4]

$$\Gamma(v) = \gamma_{e,1} + \sum_{g=1}^{G-1} \frac{1}{2}(\gamma_{e,g+1} - \gamma_{e,g})(1 + \sin(\arctan(\alpha_g(v - v_{sh,g})))) \ , \tag{2.18}$$

where $v_{sh,g}$ are the gear-shift speeds and the coefficients α_g are chosen to make the gear transition sufficiently smooth, see Fig. 2.9.

Following the backward calculation approach illustrated in Fig. 2.2, the engine torque T_e is related to the powertrain force F_p through the overall transmission ratio,

$$T_e(t) = \frac{F_p(t) r_w}{\gamma_e(t) \eta_t^{\text{sign}(F_p(t))}} \ , \tag{2.19}$$

where r_w is the wheel radius and η_t is the transmission efficiency. This quantity depends on the gear ratio used, although this dependency is often neglected.

Conversely, engine rotational speed ω_e is related to the vehicle's speed v,

[4]This approximation is usually valid only for small and large force values. For intermediate values, the gear-shift speeds would increase with force. Also, the gear-shift speeds are usually different for upshifts than for downshifts.

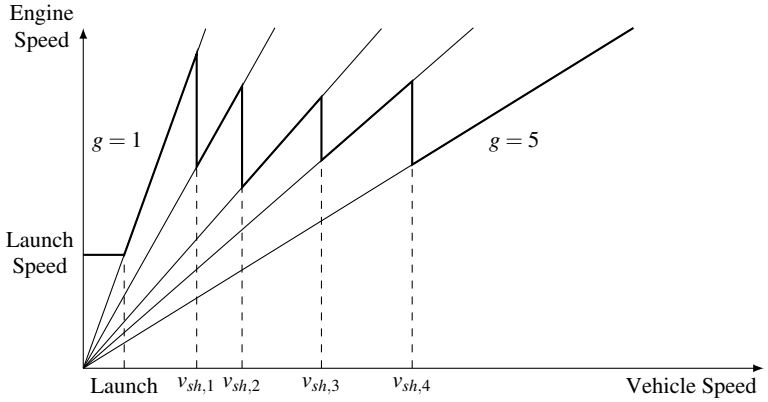

Fig. 2.9 Qualitative speed-only-dependent gear shift law described by (2.18)

$$\omega_e(t) = \frac{\gamma_e(t)}{r_w} v(t) \ . \tag{2.20}$$

Note that (2.19) implies a discontinuous derivative $\partial T_e / \partial F_p$ at $F_p = 0$ (coasting operation). A particular case of coasting is when the transmission is in the neutral state, with a clutch opening to disconnect the engine from the wheels. Commonly reserved for the stopped vehicle state, this operation is nowadays used also in *sailing* maneuvers, aimed at prolonging coasting by suppressing the engine brake effect to save fuel. The neutral cannot be described by setting $\gamma_e = 0$ in (2.19) and (2.20). In this case the engine is either stopped or idling (see below).

Note also that, during clutching maneuvers (in manual transmissions) or torque converter maneuvers (in automated transmissions), the relation between engine and vehicle speeds and torques cannot be described by (2.19)–(2.20).

2.2.2 *Engine*

Although engines can differ substantially concerning the type of fuel (gasoline, diesel, alternative fuels such as LPG, natural gas, E85), the thermodynamic cycle followed (four-strokes, two-strokes), the aspiration method (naturally aspirated, supercharged), and generally the technology used, they share a similar representation for our purposes.

The fuel power P_f can be modeled under a steady-state approximation using tabulated data ("engine map") as a function of engine torque and rotational speed,

$$P_f(t) = f(T_e(t), \omega_e(t)) \ . \tag{2.21}$$

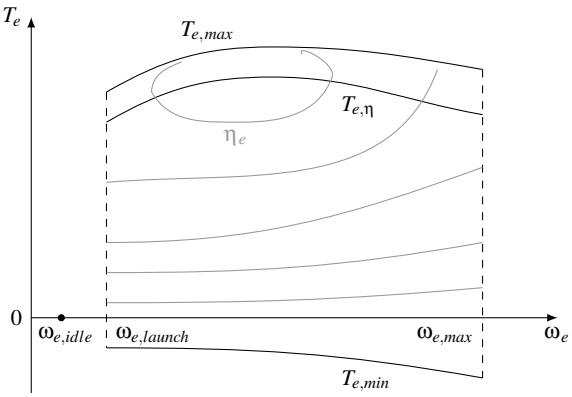

Fig. 2.10 Example efficiency map of a naturally-aspirated spark-ignition engine

Equivalently, an engine map can be expressed in terms of efficiency

$$\eta_e \triangleq \frac{T_e \omega_e}{P_f} \,, \tag{2.22}$$

as depicted by the contour lines in Fig. 2.10.

This figure also shows that the engine operation is restricted by a certain number of limitations, namely: (i) the full-load torque $T_{e,max}$, which depends on the rotational speed; (ii) the fuel-cutoff torque $T_{e,min}$, which is negative due to friction and also dependent on speed; (iii) the maximum speed $\omega_{e,max}$; and (iv) the launch speed at which the engine starts producing stable torque, $\omega_{e,launch}$.

When the vehicle is stopped or coasting, the engine might be disconnected by putting the transmission in neutral, and run at the idle speed $\omega_{e,idle}$. To cover this situation, the idle consumption must be considered alongside the engine map. However, modern engines are often equipped with a stop-start device that turns the engine off during these operations.

The curve $T_{e,\eta}$ is the locus of the engine operating points for which the efficiency—defined by (2.22)—is the highest for those at the same output power. It is referred to as optimal operating line (OOL) of the engine and does not in general coincide with the maximal torque curve.

For the online applications described later in this book, e.g., in Chap. 8, approximated polynomial expressions are preferred to (2.21). The most used of such expressions is the affine-in-torque Willans model [1]

$$P_f(t) = \frac{T_e(t)\omega_e(t) + P_{e,min}(\omega_e(t))}{e(\omega_e(t))} \,, \tag{2.23}$$

defined by the speed-dependent parameters e (efficiency of the thermodynamic energy conversion from fuel to cylinder pressure) and $P_{e,min} = \omega_e T_{e,min}$ (mechan-

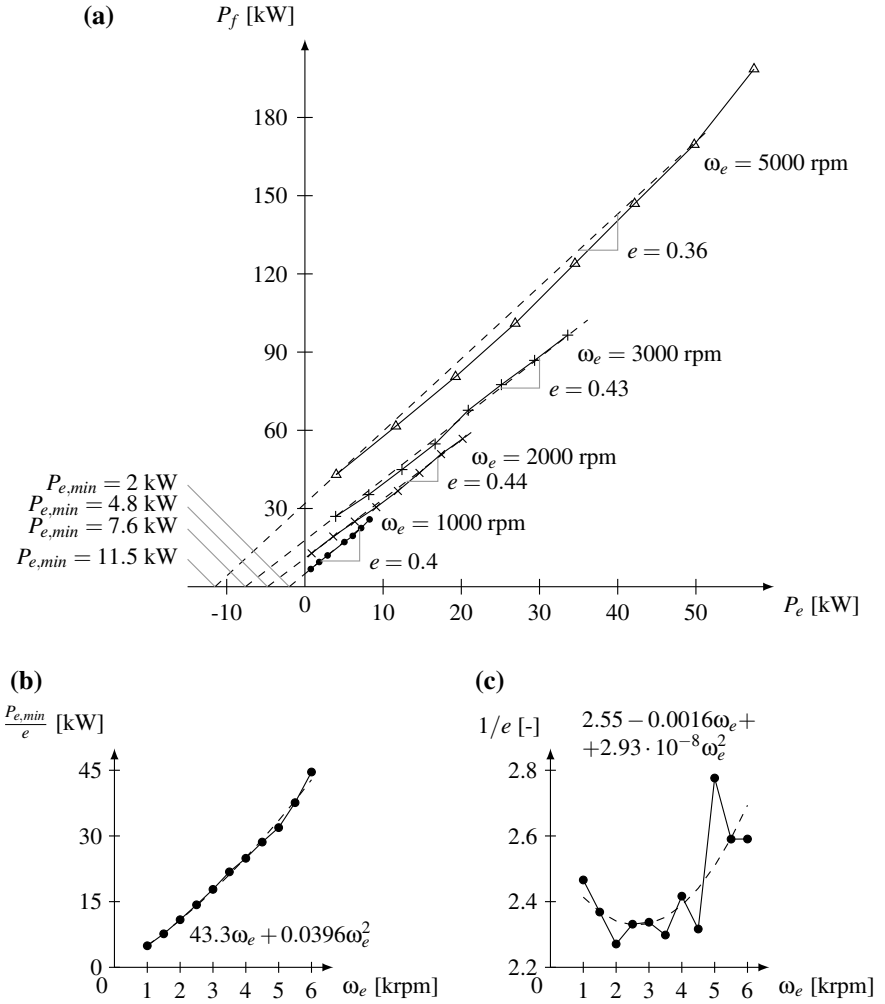

Fig. 2.11 Willans lines (dashed) and actual map data (solid marked) of a naturally-aspirated spark-ignition engine, with fitted values of e and $P_{e,min}$ for various speeds (**a**). Parametrization of $P_{e,min}/e$ (**b**) and $1/e$ (**c**) leading to (2.24) (ω_e in rad/s)

ical friction and pumping losses). An example Willans representation of an engine map is shown in Fig. 2.11a.

The further parametrization of the terms $1/e$ and $P_{e,min}/e$ as a function of speed leads to the closed-form expression [7]

$$P_f(t) = (k_{e,0}\omega_e(t) + k_{e,1}\omega_e^2(t)) + (k_{e,2} + k_{e,3}\omega_e(t) + k_{e,4}\omega_e^2(t))T_e(t)\omega_e(t) \ , \tag{2.24}$$

where the k_{ei}'s, $i = 0, \ldots, 4$ are design-dependent coefficients. An illustrative example of the data fitting leading to (2.24) is shown in Fig. 2.11b, c. Note that (2.23) or (2.24) also capture the idle speed consumption, obtained by setting $T_e = 0$ and $\omega_e = \omega_{e,idle}$.

In the example of Fig. 2.11, the affine dependency of the fuel power on torque or mechanical power is reasonably valid for all speeds shown, and up to the maximal torque allowed at each speed. In more general terms, however, the affine range extends only up to an intermediate torque, often coincident with or close to $T_{e,\eta}$, after which the curve $P_f - P_e$ becomes visibly convex.[5]

The engine brake torque curve $T_{e,min}(\omega_e)$ is obtained from (2.24) by setting $P_f = 0$ (fuel cutoff). For the maximum torque curve $T_{e,max}$, convenient parametrizations [7] are the quadratic relation

$$T_{e,max}(t) = k_{e,5} + k_{e,6}\omega_e(t) + k_{e,7}\omega_e^2(t) \tag{2.25}$$

for SI, naturally-aspirated engines, and a piecewise-affine relation of the type

$$T_{e,max}(t) = \min\left(k_{e,8} + k_{e,9}\omega_e(t), k_{e,10}, k_{e,11} + k_{e,12}\omega_e(t)\right) \tag{2.26}$$

for turbocharged engines.

2.2.3 *Fuel Energy Consumption of ICEVs*

With the models introduced in the previous sections, it is possible to evaluate the fuel energy consumption of an ICEV defined by (2.16). It is further assumed that in the braking phase $\mathcal{B}$ ($F_w < 0$) the fuel injection is disabled (*fuel cut-off*), thus the engine absorbs the power $P_{e,min}$ (engine brake). With the notation of Sect. 2.1.3, $k_b = -P_{e,min}\eta_t/(vF_w)$. Consequently, the integral in (2.16) is limited to the traction phase and, inserting (2.23), is evaluated as

$$E_T^{(ICEV)} = \int_{\mathcal{T}} \frac{v(t)F_w(t)/\eta_t + P_{e,min}(\omega_e(t))}{e(\omega_e(t))}\, dt\ , \tag{2.27}$$

With the parametrization of (2.24), the integral in (2.27) can be written as a sum of terms

$$\begin{aligned} E_T^{(ICEV)} = \sum_g E_{T,g}^{(ICEV)} = \sum_g \int_{\mathcal{T}_g} &\left(k_{e,0}\omega_{e,g}(t) + k_{e,1}\omega_{e,g}^2 + \right. \\ &+ \left.\left(k_{e,2} + k_{e,3}\omega_{e,g}(t) + k_{e,4}\omega_{e,g}^2(t)\right) v(t)F_w(t)/\eta_t\right) dt\ , \end{aligned} \tag{2.28}$$

[5] A behavior that is seen for the last point at 5000 rpm in Fig. 2.11a. For some engine technologies, e.g., downsized-supercharged engines that require spark retard to avoid knock at high torque, these curves might become more convex at high engine power, especially at low speed.

where each term $E_{T,g}^{(ICEV)}$ corresponds to the gear g and is evaluated by integrating over $\mathcal{T}_g$, the particular portion of $\mathcal{T}$ where gear g is engaged. Developing all terms, an explicit formula is obtained, which reads

$$\begin{aligned} E_{T,g}^{(ICEV)} = & \left(\frac{k_{e,0}\gamma_{e,g}}{r_w} + \frac{k_{e,2}C_0}{\eta_t}\right)\int_{\mathcal{T}_g} v(t)dt + \\ & \left(\frac{k_{e,1}\gamma_{e,g}^2}{r_w^2} + \frac{k_{e,2}C_1}{\eta_t} + \frac{k_{e,3}C_0\gamma_{e,g}}{r_w\eta_t}\right)\int_{\mathcal{T}_g} v^2(t)dt + \\ & \left(\frac{k_{e,2}C_2}{\eta_t} + \frac{k_{e,3}\gamma_{e,g}C_1}{r_w\eta_t} + \frac{k_{e,4}\gamma_{e,g}^2C_0}{r_w^2\eta_t}\right)\int_{\mathcal{T}_g} v^3(t)dt + \\ & \left(\frac{k_{e,3}\gamma_{e,g}C_2}{r_w\eta_t} + \frac{k_{e,4}\gamma_{e,g}^2C_1}{r_w^2\eta_t}\right)\int_{\mathcal{T}_g} v^4(t)dt + \left(\frac{k_{e,4}\gamma_{e,g}^2C_2}{r_w^2\eta_t}\right)\int_{\mathcal{T}_g} v^5(t)dt + \\ & \left(\frac{m_t k_{e,2}}{\eta_t}\right)\int_{\mathcal{T}_g} v(t)dv + \left(\frac{m_t k_{e,3}\gamma_{e,g}}{r_w\eta_t}\right)\int_{\mathcal{T}_g} v^2(t)dv + \\ & \left(\frac{m_t k_{e,4}\gamma_{e,g}^2}{r_w^2\eta_t}\right)\int_{\mathcal{T}_g} v^3(t)dv \end{aligned} \tag{2.29}$$

In this formulation, the fuel energy consumption is expressed as a sum of many terms, each being the product of a vehicle-dependent factor and a driving-dependent factor under the form of an integral. Each of these integrals can be further expressed as a function of the average speed over the partial phase $\mathcal{T}_g$ and higher moments, using the procedure illustrated in Sect. 2.1.2.

2.3 Electric Vehicles

Electric vehicles (EV) are powered by a battery that accumulates electrochemical energy and delivers electric power at its terminals. Batteries are reversible storage systems, thus they can be recharged during their operation if electricity is provided. Otherwise, they are filled back by external chargers when the vehicle is stopped at charging stations. The EV powertrain is completed by one or more reversible electric machines, that can be operated as motors or generators. Usually, three-phase alternating current machines are used. The direct-current electricity at the battery terminals is transformed to alternating current and back by a power electronic device, an *inverter*. The mechanical power at the machine shaft is linked to the wheels by the drivetrain.

In EVs, the tank energy corresponds to the electrochemical energy drained from or supplied to the battery,

$$E_T^{(EV)} = \int_0^{t_f} P_b(t)dt \ , \tag{2.30}$$

where P_b is the electrochemical power. How this quantity is related to the driving profile, will be now described by following the approach of Fig. 2.3 and analyzing separately the drivetrain, the motor with its inverter, the power link, and the battery.

2.3.1 Drivetrain

In electric vehicles the drivetrain is usually equipped with a transmission with a fixed configuration (single-gear reductor). Defining the drivetrain transmission ratio γ_m as the product of the final drive and reductor ratios, (2.19)–(2.20) are replaced by

$$T_m(t) = \frac{F_p(t) r_w}{\gamma_m \eta_t^{sign(F_p(t))}} \tag{2.31}$$

and

$$\omega_m(t) = \frac{\gamma_m}{r_w} v(t) \ , \tag{2.32}$$

respectively, where T_m and ω_m are motor torque and speed.

2.3.2 Motor and Inverter

Traction motors adopted in electric vehicles are usually permanent-magnet, synchronous AC machines or, to a lesser extent, induction (asynchronous) AC machines, although newer technologies are emerging. For our purposes, all these motor types share a similar representation.

Electric power supplied to or generated by the motor, including its inverter, P_m, is usually tabulated ("motor map") as a function of motor torque and rotational speed,

$$P_m(t) = f(T_m(t), \omega_m(t)) \ , \tag{2.33}$$

Equivalently, a motor map can be expressed in terms of efficiency

$$\eta_m \triangleq \left(\frac{T_m \omega_m}{P_m} \right)^{\text{sign}(T_m)} \ , \tag{2.34}$$

as depicted by the contour lines in Fig. 2.12. Note that the motor map extends to two quadrants of the torque-speed plane, reflecting the reversible nature of these machines, that are able to operate as a motor ($T_m > 0$) as well as a generator ($T_m < 0$).

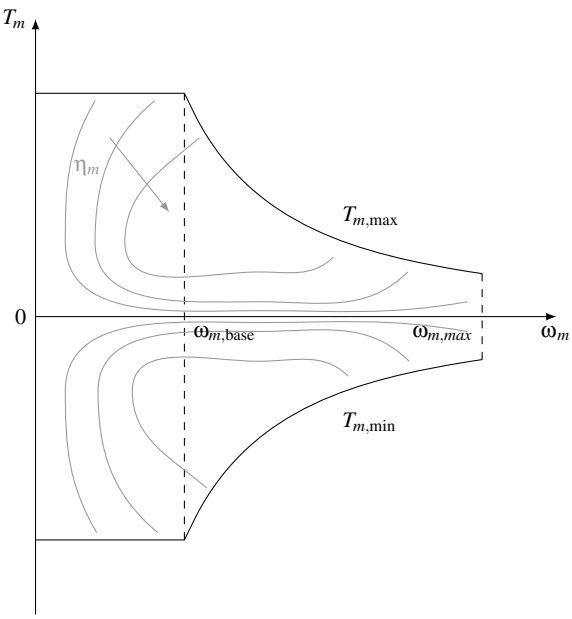

Fig. 2.12 Example efficiency map of an electric machine

The operation of electric machines is restricted by a number of limitations, namely: (i) the maximum torque $T_{m,max}$ that can be provided continuously,[6] a speed-dependent quantity that is constant from zero speed up to a certain value known as base speed, $\omega_{m,base}$, then decreases with speed roughly hyperbolically; (ii) the maximum torque in the generator range, $T_{m,min}$ that is a similar function of speed; and (iii) the maximum speed $\omega_{m,max}$. Contrarily to engines, there is no minimum speed and the motor can produce torque at rest.

For the online implementation described in Chap. 8, approximated closed-form expressions are used instead of (2.33). For instance, the physics of DC motor inspires the quadratic model [8]

$$P_m(t) = b_2(\omega_m(t))T_m^2(t) + b_1(\omega_m(t))T_m(t) + b_0(\omega_m(t)) \ , \tag{2.35}$$

where the b's are tunable parameters. Further parametrization of the b's coefficients as a function of the motor speed leads to the closed-form expression

$$\begin{aligned} P_m(t) = &\left(k_{m,4} + k_{m,5}\omega_m(t) + k_{m,6}\omega_m^2(t)\right) T_m^2(t) + \\ &+ k_{m,3}\omega_m(t)T_m(t) + k_{m,2}\omega_m^2(t) + k_{m,1}\omega_m(t) + k_{m,0} \end{aligned} \tag{2.36}$$

[6] Higher torque levels can be delivered for short times; correspondingly, motor maps often present *peak torque* curves for various delivery times.

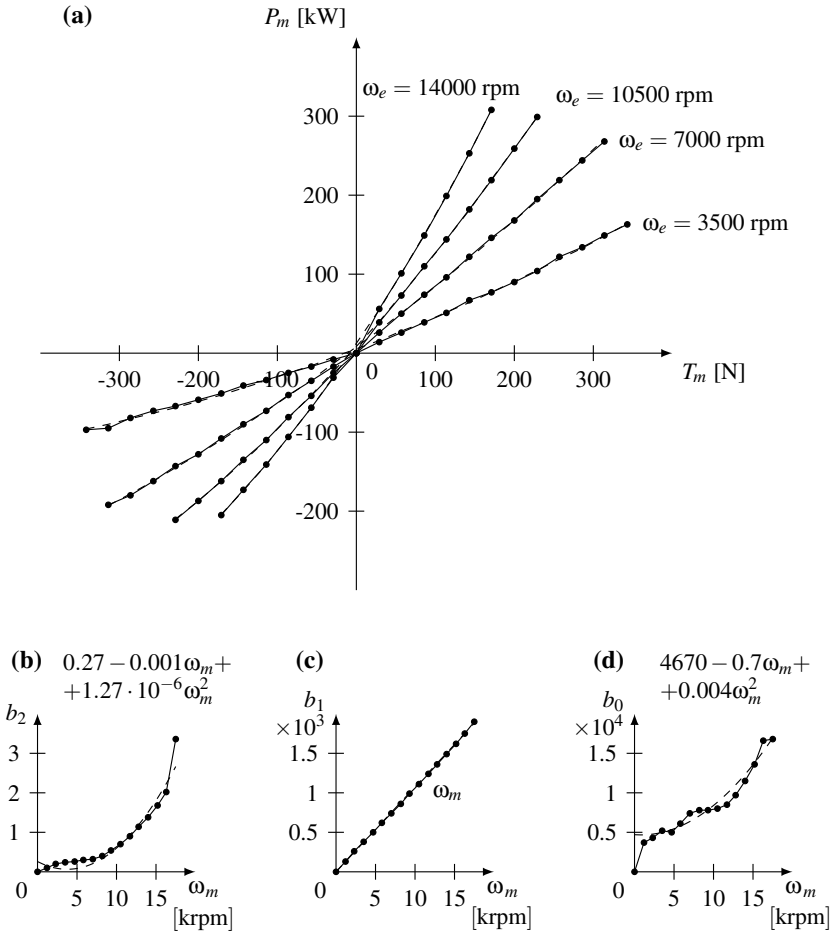

Fig. 2.13 Quadratic model (dashed) and actual map data (solid marked) of a synchronous permanent-magnet motor (**a**). Parametrization of b_2 (**b**), b_1 (**c**), and b_0 (**d**) leading to (2.36) (ω_e in rad/s)

that, as Fig. 2.13 illustrates, is often sufficiently accurate, at least in the operating regions not too far above the base speed. Even simpler representations, for instance, constant motoring and generating efficiency, have also been adopted in energy efficiency studies.

As shown in Fig. 2.12, the maximum torque curve can be effectively approximated as

$$T_{m,max}(t) = k_{m,7} \frac{\min(\omega_{m,base}, \omega_m(t))}{\omega_m(t)} \ , \tag{2.37}$$

where the coefficient $k_{m,7}$ corresponds to the nominal torque and the base speed is the ratio of nominal power to nominal torque. As for the minimum torque curve $T_{m,min}$, it is often equaled to $-T_{m,max}$.

2.3.3 Power Link

The power link electrically connects the battery terminals to the inverter input, allowing for bi-directional flow of electricity. Although losses inevitably occur in power links, usually these contributions are neglected, such that, following the backward calculation flow in Fig. 2.3, it is assumed that

$$P_l(t) = P_m(t)\,. \tag{2.38}$$

where P_l is the electric power out of the battery.

2.3.4 Battery

As of 2017, most of automotive traction batteries embody one of the variants of the lithium-ion technology, which has superseded older technologies such as nickel-metal hydride or lead-acid. Although lithium-ion batteries can differ substantially among each other concerning the specific chemistry of the cathode (NMC, LMO, LFP, LCO, NCA, etc.), the anode, and their sizes, for our purposes they share a similar representation.

The battery power is calculated by modeling the battery electro-chemistry as an equivalent electric circuit, with an ideal voltage source V_{b0} and an internal resistance R_b in series, see Fig. 2.14. With this representation, the electrochemical power to be used in (2.30) is $P_b = V_{b0} I_b$ and it is further evaluated as a function of the terminal power $P_l = V_b I_b$ as

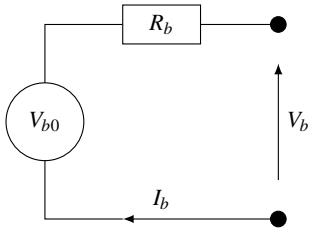

Fig. 2.14 Equivalent circuit of a battery

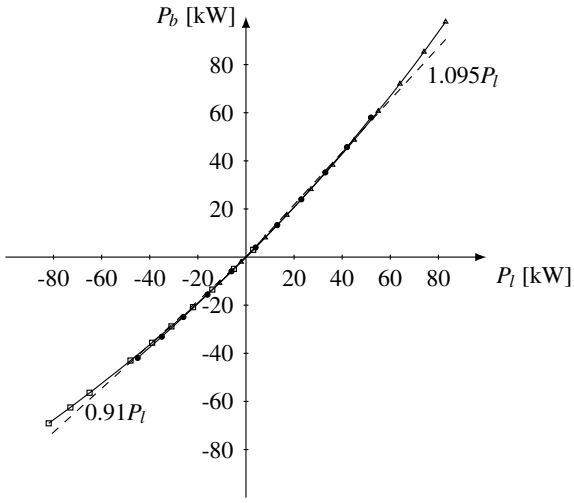

Fig. 2.15 Constant-efficiency model (dashed) and actual tabulated data (solid marked: ∗ 50% SoC, △ 90% SoC, □ 10% SoC) of a lithium-ion battery

$$P_b(t) = \frac{V_{b0}^2}{2R_b} - V_{b0}\sqrt{\frac{V_{b0}^2 - 4P_l(t)R_b}{4R_b^2}}\,. \tag{2.39}$$

Note that P_b and P_l are defined as positive for discharging and negative for charging.

The difference between P_b and P_l is due to inner battery losses. For the online use described in Chap. 7, these effects are sometimes further simplified to a constant efficiency model

$$P_b(t) = P_l(t)\eta_b^{-\mathrm{sign}(P_l(t))}\,, \tag{2.40}$$

see Fig. 2.15, or even neglected, $P_b(t) = P_l(t)$.

The open-circuit voltage V_{b0} and internal resistance R_b may actually vary with time as they depend on the level of energy accumulated in the battery. The usual measure of such energy is the State of Charge (SoC), defined as $\xi_b = q_b/Q_b$, where q_b is the remaining charge and Q_b is the nominal battery capacity, a quantity that is usually expressed in ampere-hour units (Ah). Assuming a simple "Coulomb-counting" model for the battery charge depletion, $dq_b(t)/dt = -I_b(t)$, the SoC dynamics reads

$$\dot{\xi}_b(t) = -\frac{P_b(t)}{V_{b0}Q_b}\,. \tag{2.41}$$

The SoC is useful to describe the limitations imposed on the battery operation. Of course, in principle $0 \le \xi_b \le 1$, however, automotive batteries are often managed in such a way that $\xi_{b,min} \le \xi_b \le \xi_{b,max}$, where the admissible range tends to be wider for batteries equipping EVs and plug-in HEVs. Additional operating limits are imposed on battery voltage and, consequently, on output power P_l.

We define for later use the energy stored in the battery as $\varepsilon_b \triangleq q_b V_{b0}$.

2.3.5 Electric Energy Consumption of EVs

With the models introduced in the previous sections, it is possible to evaluate the electric energy consumption of an EV. It is further assumed that friction brakes are not used so that the recuperation potential is exploited at its maximum ($k_b = 1$ in the nomenclature of Sect. 2.1.3).[7]

Since the drivetrain model (2.31) and the battery model (2.40) have a different form for traction/discharge ($T_m > 0, P_m > 0$) and braking/charge ($T_m < 0, P_m < 0$), the integral of (2.30) is conveniently split in two parts,

$$E_T^{(EV)} = \sum_{\sigma} E_{T,\sigma}^{(EV)} \ , \tag{2.42}$$

with $\sigma \in \{\mathcal{T}, \mathcal{B}\}$ spanning the two phases defined in Sect. 2.1.3. Using the parametric models (2.36) and (2.40), and developing all terms, an involved but explicit formula is obtained, of the type

$$E_{T,\sigma}^{(EV)} = \sum_{i,j,\sigma} \mathsf{E}_{ij}^{\sigma} \mathsf{C}_{ij}^{\sigma} \ . \tag{2.43}$$

Each term in the summation is the product of a vehicle-dependent factor (E) and a driving-dependent factor (C), defined as

$$\mathsf{C}_{ij}^{\sigma} \triangleq \int_{\sigma} v^i \dot{v}^j dt \ , \tag{2.44}$$

with the integral extended only to times where the mode σ is active. For instance, when $k_{m,5} = k_{m,6} = 0$ and $\eta_b = 1$, one obtains

$$\begin{aligned} E_{T,\sigma}^{(EV)} = & \left(k_{m,0} + \frac{C_0^2 k_{m,4} r_w^2}{\eta_t^{2\sigma} \gamma_m^2} \right) \int_{\sigma} dt + \left(\frac{C_0 k_{m,3}}{\eta_t^{\sigma}} + \frac{\gamma_m k_{m,1}}{r_w} + \frac{2 C_0 C_1 k_{m,4} r_w^2}{\eta_t^{2\sigma} \gamma_m^2} \right) \cdot \\ & \int_{\sigma} v(t) dt + \left(\frac{C_1 k_{m,3}}{\eta_t^{\sigma}} + \frac{\gamma_m^2 k_{m,2}}{r_w^2} + \frac{C_1^2 k_{m,4} r_w^2}{\eta_t^{2\sigma} \gamma_m^2} + \frac{2 C_0 C_2 k_{m,4} r_w^2}{\eta_t^{2\sigma} \gamma_m^2} \right) \int_{\sigma} v^2(t) dt + \\ & + \left(\frac{C_2 k_{m,3}}{\eta_t^{\sigma}} + \frac{2 C_1 C_2 k_{m,4} r_w^2}{\eta_t^{2\sigma} \gamma_m^2} \right) \int_{\sigma} v^3(t) dt + \left(\frac{C_2^2 k_{m,4} r_w^2}{\eta_t^{2\sigma} \gamma_m^2} \right) \int_{\sigma} v^4(t) dt + \\ & + \left(\frac{2 C_0 k_{m,4} m r_w^2}{\eta_t^{2\sigma} \gamma_m^2} \right) \int_{\sigma} a(t) dt + \left(\frac{k_{m,3} m}{\eta_t^{\sigma}} + \frac{2 C_1 k_{m,4} m r_w^2}{\eta_t^{2\sigma} \gamma_m^2} \right) \int_{\sigma} v(t) a(t) dt + \\ & + \frac{2 C_2 k_{m,4} m r_w^2}{\eta_t^{2\sigma} \gamma_m^2} \int_{\sigma} a(t) v^2(t) dt + \left(\frac{k_{m,4} m^2 r_w^2}{\eta_t^{2\sigma} \gamma_m^2} \right) \int_{\sigma} a^2(t) dt \ , \end{aligned} \tag{2.45}$$

where the exponents σ's stand here for $+1$ (traction) and -1 (braking), respectively.

[7] In practice the situation $k_b < 1$ is common, since in most braking maneuvers both vehicle axles must brake due to stability issues, and often recuperation is available only on one axle.

Each of these integrals can be further expressed as a function of the average speed and higher moments over the phases $\mathcal{T}$ and $\mathcal{B}$, using the procedure illustrated in Sect. 2.1.2.

2.4 Hybrid-Electric Vehicles

Hybrid-electric vehicles (HEV) are a combination of an engine-based vehicle and an electric vehicle. According to how the power is combined, HEVs are classified as *parallel* (coupling of the mechanical power of the engine with that of the motor), *series* (coupling of the electric power of the battery and of an engine-based electrical generation unit), or *series-parallel* (both couplings are present, often with a power-split device such as a planetary gear-set). According to the position of the coupling, parallel hybrids are further classified to several types, typically labeled from P0, if the motor is coupled to the engine belt, to P4, if the motor is mounted on one of the axles. According to the battery operation strategy, HEVs are classified as charge-sustaining hybrids, where the battery cannot be recharged from an external source, or plug-in hybrids.

In HEVs, energy is generally drained both from the fuel tank and the battery. The measure of energy consumption adopted depends on the type of battery operation. However, a common definition of an HEV energy consumption can be written as

$$E_T^{(HEV)} = \int_0^{t_f} (P_f(t) + s \cdot P_b(t))dt \ , \tag{2.46}$$

where s is an "equivalence factor" that weights the electricity consumption with respect to the fuel consumption.

For charge-sustaining HEVs, s is vehicle- and cycle-dependent and must be determined by interpolation of two or more tests, e.g., using the procedure [9]. For plug-in hybrids, standards such as [9] recommend fuel economy evaluation rules that can be transcribed as (2.46), where s is a prescribed coefficient.

How the quantities P_f and P_b are related to the driving profile, will be now described by following the approach of Figs. 2.4 and 2.5. Models of the engine, the electric machine, and the battery presented in the previous sections still apply to HEVs. However, the nature and role of drivetrain and power link depends on the hybrid architecture, as will be now discussed.

2.4.1 Drivetrain and Power Link

In parallel HEVs the powertrain force results from the combination of the engine torque and the motor torque,

$$
\begin{aligned}
T_e(t) &= u(t)\frac{F_p(t)r_w}{\gamma_e(t)\eta_t^{\text{sign}(F_p(t))}} \ , \\
T_m(t) &= (1-u(t))\frac{F_p(t)r_w}{\gamma_m\eta_t^{\text{sign}(F_p(t))}} \ ,
\end{aligned}
\tag{2.47}
$$

where $u(t)$, the *torque split ratio*, is the degree of freedom offered by the parallel hybrid architecture. In other terms, one between T_e and T_m can be chosen freely to satisfy a given F_p. In contrast, the speed levels are unambiguously related to the vehicle speed,

$$
\begin{aligned}
\omega_m(t) &= \frac{\gamma_m}{r_w}v(t) \ , \\
\omega_e(t) &= \frac{\gamma_e(t)}{r_w}v(t) \ .
\end{aligned}
\tag{2.48}
$$

As for the power link, in parallel HEVs it links a single electric source (battery) to a single electric load (motor), therefore (2.38) applies.

In series hybrids, the drivetrain is described by (2.31) and (2.32), while the power balance at the electric link reads

$$
\begin{aligned}
P_g(t) &= u(t)P_m(t) \ , \\
P_l(t) &= (1-u(t))P_m(t) \ ,
\end{aligned}
\tag{2.49}
$$

where $u(t)$ is now the *power split ratio*, a degree of freedom offered by the series architecture, and P_g is the electric power generated by the auxiliary power unit (APU).

This electric generation unit is composed of an engine and an electric machine, the latter exclusively operated as a generator, mechanically connected such that T_e is rigidly tied to T_g and so are ω_e and ω_g. For such a system, the relation between $P_f(t)$ and $P_g(t)$ is not unambiguous, as it depends on the rotational speed at which the two machines are operated. The latter is a second degree of freedom offered by the series architecture and is usually chosen such as to maximize the APU efficiency, following the optimal operating line of the APU (Fig. 2.16). This curve ultimately provides the speeds and torques as a function of the generated electric power P_g, while the engine models of Sect. 2.2.2 eventually provide P_f.

In series-parallel HEVs, coupling relations are more complex than (2.47)–(2.49), as they involve coupling of rotational speeds. The reader is therefore referred to standard vehicle modeling books [1].

The role of determining the degree of freedom $u(t)$, either torque or power split, or even more complex combination for architectures not detailed here, is played by the hybrid energy management strategy (EMS). A description of such a strategy is therefore necessary in order to predict the fuel and electric consumption of a HEV for a given driving profile.

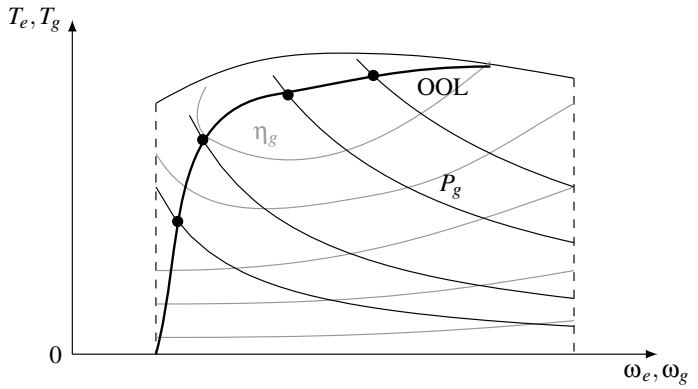

Fig. 2.16 Example optimal operating line (OOL) of an APU. Also shown are contour lines of P_g: the OOL is the locus of points that maximize η_g for different values of P_g

2.4.2 Energy Management Strategy

Several control designs are used for the EMS, including heuristic strategies and optimization-based strategies.

Heuristic EMS are based on predefined rules of the type

$$u(t) = f\left(F_p(t), v(t), \xi_b(t), \gamma_e(t), \theta_e(t), \ldots\right) , \tag{2.50}$$

where the arguments in the right-hand side of (2.50) describe the vehicle state and the driver's request. The function $f(\cdot)$ is implemented in the onboard control unit under the form of look-up tables, algorithms, or finite-state machines. As an example, in a parallel HEV these rules might prescribe the use of the purely electric mode ($u = 0$) only under certain driving situations, typically low speed and acceleration, and for sufficiently high SoC. Heuristic strategies are heavily dependent on threshold values or maps, which are to be tuned point by point with a relevant calibration effort.

Alternatively, optimal EMS are inspired by the solution of an optimal control problem that aims to minimize the fuel consumption over the horizon t_f, under a constraint over the battery state of charge at the end of the horizon. In mathematical terms,

$$\min_{u(t)} \int_0^{t_f} P_f(u, v(t), \ldots) dt , \tag{2.51}$$

with $u(t)$ subject to all physical limits described in the previous sections, and such that

$$\int_0^{t_f} P_b(u(t), v(t), \ldots) dt = \Delta E_b , \tag{2.52}$$

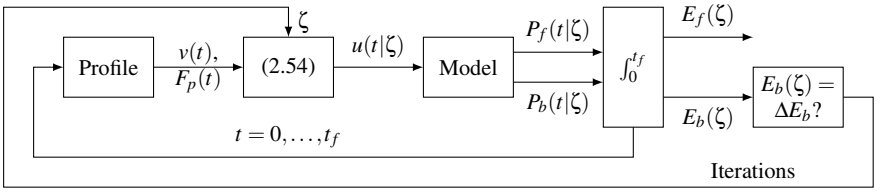

(a) Offline

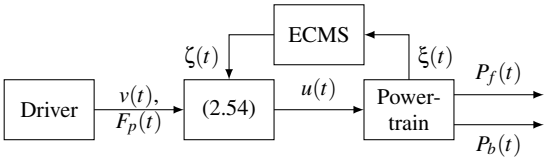

(b) Online

Fig. 2.17 Schematic flowcharts of offline and online optimal EMS

where ΔE_b is the target electric consumption. Generally, $\Delta E_b = 0$ for charge-sustaining HEVs, while it is often taken as the remaining useful energy in the battery for plug-in hybrids, in such a way that the EMS provides full discharge at the end of the trip with minimum fuel consumption.

Using the theory of optimal control, this problem is solved by forming a Hamiltonian function H and then finding $u(t)$ such that

$$u(t) = \arg\min H(u, v(t), \ldots) \tag{2.53}$$

$$H(u, v(t), \ldots) = P_f(u, v(t), \ldots) + \zeta^* P_b(u, v(t), \ldots) \, . \tag{2.54}$$

The quantity ζ^* is determined as the particular value that, when applied in (2.54), gives place to trajectories $u(t|\zeta^*)$ and consequently $P_f(t|\zeta^*)$, $P_b(t|\zeta^*)$, that fulfill (2.52). As such, ζ^* is a vehicle-dependent constant that is additionally a function of the whole profile $v(t)$, $t \in [0, t_f]$. It can be found by iterations for a prescribed driving profile known in advance ("offline optimal EMS"), see Fig. 2.17a.

However, the optimal ζ^* is generally not predictable during a real operation, since the future driving profiles are generally not known in advance. Therefore, online EMS can only be sub-optimal by adopting some kind of rule to provide estimations $\zeta(t)$ of ζ as time advances. Often the *Equivalent Consumption Minimization Strategy* (ECMS) approach is used, where $\zeta(t)$ is regulated as a function of deviations of SoC from its target value, see Fig. 2.17b.

The use of connectivity in CAVs and conventional vehicles can improve the estimation of ζ^* and thus the optimality of the EMS, by anticipating the fact that future road slopes and traffic conditions will lead to an over- or under-usage of the battery. The resulting *predictive energy management strategies* are currently a subject of research [10] but won't be treated further in this book.

2.4.3 Energy Consumption of HEVs

A closed-form expression of the energy consumed by an HEV along a given driving profile is harder to obtain than for ICEVs or EVs, even with suitable approximations for P_f and P_b, because of the fundamental role played by the energy management strategy in defining such consumption. In particular, if the minimal fuel consumption is to be predicted, that would imply an iterative process to find the optimal ζ^*.

The method called *fully-analytical consumption estimation* (FACE) [7] is based on the assumption, confirmed by observation, that the overall consumption (2.46) is only slightly dependent on the particular choice of ζ, if an optimal EMS (2.54) based on this value is applied. Under this assumption, any "reasonable" value of ζ would provide a good estimate of the overall energy consumption (2.46).[8] A reference value can, for instance, be evaluated "offline" for a known driving profile, then applied in (2.46) to evaluate the energy consumption of any other profile, even if ζ does not satisfy condition (2.52).

According to this method, an estimation of the energy consumed is thus

$$E_T^{(HEV)} = \int_0^{t_f} P_f(t|s)dt + \zeta \int_0^{t_f} P_b(t|s)dt \ . \tag{2.55}$$

Using the models and methods already illustrated for ICEVs and EVs, (2.55) can be reorganized as

$$E_T^{(HEV)} = \sum_{i,j,g,\sigma} \mathsf{F}_{ij}^{g\sigma} \mathsf{C}_{ij}^{g\sigma} + \zeta \sum_{i,j,g,\sigma} \mathsf{E}_{ij}^{g\sigma} \mathsf{C}_{ij}^{g\sigma} \ , \tag{2.56}$$

that is, a sum of many terms, each being the product of a vehicle-dependent factor (F or E) and a driving-dependent factor (C). The latter are defined as

$$\mathsf{C}_{ij}^{g\sigma} \triangleq \int_{g,\sigma} v^i \dot{v}^j dt \ , \tag{2.57}$$

with the integral extended only to times when the gear g and the mode σ are active.

Note that (2.29) and (2.43) are particular cases of (2.56). However, in HEVs the set of possible operating modes is larger than in ICEVs or EVs, where $\sigma \in \{\mathcal{T}, \mathcal{B}\}$, since it may include a fully-electric mode ($u = 0$), a fully-ICE mode ($u = 1$), a "boost" mode ($0 < u < 1$), a recharge mode ($u > 1$), etc. Additionally, how a given profile is split into the various modes also depends on ζ.

[8] Only the overall, or "equivalent", consumption can be estimated with this method; it does not allow to find separately the two energy contributions, i.e., the minimal fuel consumption for a given battery consumption.

2.5 Human-Powered Vehicles (Bicycles)

The most common human-powered vehicles (HPV) are bicycles. We shall thus limit our analysis to such systems, where the powertrain is usually composed of the cyclist, pedals, and a chain transmission. Besides purely-human-powered bicycles, motorized bicycles also exist. While this concept has been historically dominated by engine-based designs, today an increasingly greater role is played by *electric bicycles*, which assist the cyclist with integrated electric motor and battery. Electric bicycles are further classified as *pedal-assist*, where the motor augments the efforts of cyclists when a sensor detects that they are pedaling, and *power-on-demand* systems (sensorless), where the motor is activated by a throttle. The European legislation limits the electric assistance at 250 W and up to 25 km/h speed. Those pedal-assist systems that exceed these limits (e-bikes or s-pedelecs) are usually legally classed as motorcycles.

The human body is (also) a power converter that takes energy through food and drink and produces useful energy in the form of muscular movements. The "tank" energy of a bicycle is thus defined as the metabolic energy spent by the cyclist,

$$E_T^{(HPV)} = \int_0^{t_f} P_h(t)dt \ , \tag{2.58}$$

where P_h is the *metabolic power*, usually defined with respect to the oxygen uptake, that is, as the product of the volumetric consumption rate and the energy density of oxygen.

How this quantity is related to the cycling profile will be now described by following the approach of Fig. 2.6 and analyzing separately the drivetrain and the cyclist's physiology.

2.5.1 Drivetrain

For a discrete-gear chain transmission, the force exerted by cyclist on pedals is evaluated as a function of the needed force at wheels as

$$F_c(t) = \frac{1}{\gamma_t(t)\eta_t}\frac{r_w}{l_c}F_p(t) \ , \tag{2.59}$$

where γ_t is the chosen transmission ratio, η_t its efficiency (supposed constant), r_w is the wheel radius, l_c the crank arm length. The *cadence*, or pedal rotational speed, is

$$\omega_c(t) = \frac{\gamma_t(t)v(t)}{r_w} \ . \tag{2.60}$$

Consequently, the mechanical power is $P_c = T_c\omega_c = F_c l_c \omega_c$.

For electric bicycles, (2.59) is replaced by

$$F_c(t) = u(t)\frac{1}{\gamma_t(t)\eta_t}\frac{r_w}{l_c}F_p(t) \ , \tag{2.61}$$

where $u(t)$ is the power split ratio, while the motor power is

$$P_m(t) = (1 - u(t))\frac{v(t)F_p(t)}{\eta_t} \ . \tag{2.62}$$

For pedal-assist electric bicycles (pedelecs), $u(t)$ is constant and determined by design. For power-on-demand electric bicycles, the determination of $u(t)$ is the role of an energy management strategy, similarly to HEVs. However, in this case, u is usually not a continuous variable but can be chosen only among a discrete set of values.

2.5.2 Cyclist

The evaluation of the oxygen consumption as a function of the cycling conditions is a complex subject that lacks a general and widely accepted model. Some simple equations could be nevertheless found in the specialized physiology literature [11–15].

The conversion from the metabolic power to the mechanical power is the result of two pathways to produce ATP (adenosine triphosphate), the energy carrier to the muscles: *aerobic* and *anaerobic*. The former is a process that takes place in the presence of oxygen and is thus associated with oxygen uptake. In contrast, the anaerobic pathway depletes stored resources, leading to lactate formation whose accumulation in the muscles generates feelings of fatigue and exhaustion. While the aerobic pathway is characterized by unlimited available energy but finite power capability, the anaerobic pathway is characterized by larger power but finite energy, thus it is available only for short times.

Under quasi-stationary conditions, the anaerobic pathway is not active and the oxygen uptake is a function of the power exerted and the pedaling cadence. This dependency can be expressed with a Willans-type model,

$$P_h(t) = \frac{P_c}{e_h(\omega_h(t))} + P_{h,0}(\omega_h(t)) \ , \tag{2.63}$$

where $P_{h,0}$ is the metabolic power with cyclist freewheeling (zero-work) and e_h the net efficiency [11]. These parameters are subject-dependent but experimental tests suggest that on average they both increase with the pedaling cadence. Consequently, the (gross) cycling efficiency

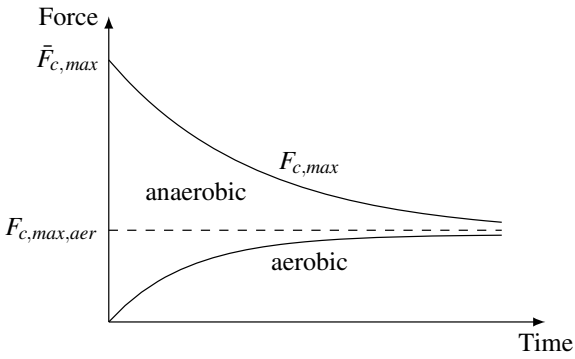

Fig. 2.18 Illustration of the various mechanisms leading to the maximum force exerted by the cyclist. Area between the curves $F_{c,max}$ and $F_{c,max,aer}$ is proportional to the anaerobic work capacity AWC

$$\eta_h \triangleq \frac{P_c}{P_h} \tag{2.64}$$

is a function that increases with power but decreases with cadence. Typical values of η_h do not exceed 20%.

The maximum power that can be generated under stationary conditions, $P_{h,max}$, is proportional to the maximum oxygen uptake (also known as $\dot{V}_{O_2,max}$) and often called anaerobic threshold or *critical power* (CP). However, as Fig. 2.18 suggests, this limit power is not instantaneously available from the aerobic pathway, while, on the other hand, it can be exceeded for a limited amount of time by consuming the reserves in the anaerobic pathway. This limited energy reservoir is often called anaerobic work capacity (AWC).

A general result of these processes is that, contrarily to engines or electric machines,[9] the maximal force that can be generated, $F_{c,max}$, varies with time as the effort above the CP progresses, see Fig. 2.18. This phenomenon is generally called *fatigue*. If the effort falls below the CP or ceases, the stored energy is replenished by the aerobic pathway. A simple model that describes such effects, adapted from [16], is

$$\frac{dF_{c,max}(t)}{dt} = \begin{cases} -k_{fat}\left(F_{c,max}(t) - F_{c,max,aer}\right), & \text{if } F_c \geq F_{c,max,aer} \\ k_{rec}\left(\bar{F}_{c,max}(t) - F_{c,max}\right), & \text{otherwise} \end{cases}, \tag{2.65}$$

where k_{fat} and k_{rec} are two subject-dependent coefficients, while $\bar{F}_{c,max}$ is the maximum force that an individual can develop from rest, also known as *maximum voluntary contraction* (MVC). The model (2.65) clearly captures the experimental observations that the drop of $F_{c,max}$ below MVC is quasi-exponential in time, and that the recovery mechanism tends to bring $F_{c,max}$ back to the MVC.

[9] As it was mentioned in Sect. 2.3.2, electric motors can actually deliver extra torque for short periods of time before thermal limitations are reached, and this is also true for some engines, particularly turbocharged ones. Although their time constants is much smaller, these processes could be described similarly to (2.65).

The coefficients k_{fat} and k_{rec} are physically related to the conservation of the available anaerobic energy AWC. Experimental observation suggests that k_{fat} increases with the relative force ratio $(F_c - F_{c,max,aer})/\bar{F}_{c,max}$. Correspondingly, the *maximum endurance time* (MET), i.e., the time at which $F_{c,max} = F_c$ after having applied a constant F_c, which is roughly proportional to the time constant of (2.65) and thus to $1/k_{fat}$, decreases with the relative force ratio [17].

Since the drop of $F_{c,max}$ described by (2.65) is an effect of fatigue accumulation, a measure of the fatigue level has been naturally proposed in [16] as

$$\xi_h(t) = \frac{\bar{F}_{c,max} - F_{c,max}(t)}{\bar{F}_{c,max} - F_{c,max,aer}} \,. \tag{2.66}$$

In analogy to battery SoC, the ratio ξ_h is often called *state of fatigue* (SoF).

2.5.3 Cycling Profiles

There is limited literature on behavioral models of cyclists. The model proposed in [18] consists of a parametrization of the cyclist power as a function of speed, $P_c(t) = f(v(t))$. This model is based on the assumption that cyclists preferably ride at constant nominal power, rather than at constant speed. The nominal power equals the power needed to cruise (zero acceleration) at a certain "comfort" speed on a flat terrain. Above the comfort speed, cyclists stop pedaling, while above a higher "feared" speed (that might be reached on steep downhills), they brake. In contrast, as the speed falls below a minimum speed (typically, at steep uphills), cyclists exert a power higher than the nominal.

The cycling speed and power profile could in principle be optimized along a trip, in particular for electric bikes. The optimization objective could be related to the cyclist's and the electric consumption. However, this concept is not adequately documented in the literature and won't be treated further in this book.

References

1. Guzzella L, Sciarretta A (2013) Vehicle propulsion system
2. Rill G (2011) Road vehicle dynamics: fundamentals and modeling. CRC Press
3. Kobayashi T, Sugiura H, Ono E, Katsuyama E, Yamamoto M (2016) Efficient direct yaw moment control of in-wheel motor vehicle. In: Proceedings of international symposium on advanced vehicle control
4. Wolf-Heinrich H (2013) Aerodynamics of road vehicles: from fluid mechanics to vehicle engineering. Elsevier
5. Bonnet C, Fritz H (2000) Fuel consumption reduction in a platoon: experimental results with two electronically coupled trucks at close spacing. Technical report, SAE technical paper

6. Kubička M, Klusáček J, Sciarretta A, Cela A, Mounier H, Thibault L, Niculescu S-I (2016) Performance of current eco-routing methods. In: Proceeding of intelligent vehicles symposium (IV), pp 472–477. IEEE
7. Zhao J, Sciarretta A (2017) A fully-analytical fuel consumption estimation for the optimal design of light-and heavy-duty series hybrid electric powertrains. Technical report, SAE technical paper
8. Dib W, Serrao L, Sciarretta A (2011) Optimal control to minimize trip time and energy consumption in electric vehicles. In: Proceedings of vehicle power and propulsion conference (VPPC), pp 1–8. IEEE
9. Hybrid-EV Committee et al (2010) Recommended practice for measuring the exhaust emissions and fuel economy of hybrid-electric vehicles, including plug-in hybrid vehicles. SAE International
10. Kermani S, Delprat S, Guerra T-M, Trigui R, Jeanneret B (2012) Predictive energy management for hybrid vehicle. Control Eng Pract 20(4):408–420
11. Chavarren J, Calbet JAL (1999) Cycling efficiency and pedalling frequency in road cyclists. Eur J Appl Physiol Occup Physiol 80(6):555–563
12. Morton RH (2006) The critical power and related whole-body bioenergetic models. Eur J Appl Physiol 96(4):339–354
13. Olds TS, Norton KI, Craig NP (1993) Mathematical model of cycling performance. J Appl Physiol 75(2):730–737
14. Hettinga FJ et al (2008) Optimal pacing strategy in competitive athletic performance. PhD thesis, PrintPartners Ipskamp
15. Rosero N, Martinez JJ, Leon H (2017) A bio-energetic model of cyclist for enhancing pedelec systems. IFAC-PapersOnLine 50(1):4418–4423
16. Fayazi SA, Wan N, Lucich S, Vahidi A, Mocko G (2013) Optimal pacing in a cycling time-trial considering cyclist's fatigue dynamics. In: Proceedings of American control conference (ACC), pp 6442–6447. IEEE
17. Ma L, Chablat D, Bennis F, Zhang W (2009) Dynamic muscle fatigue evaluation in virtual working environment. arXiv:0901.0222
18. Goussault R, Chasse A, Lippens F (2017) Model based cyclist energy prediction. In: Proceedings of international conference on intelligent transportation systems (ITSC), pp 1–6. IEEE